Comprehensive Modeling and Measurement of the Control Influence on Impedance at Critical LCL Frequencies for a 50 kHz SiC Converter

1st Dominik Schulz
Institute of Electrical Engineering (ETI)
Karlsruhe Institute of Technology (KIT)
Karlsruhe, Germany
dominik.schulz@kit.edu

2nd Rüdiger Schwendemann
Institute of Electrical Engineering (ETI)
Karlsruhe Institute of Technology (KIT)
Karlsruhe, Germany
ruediger.schwendemann@kit.edu

3rd Andreas Liske
Institute of Electrical Engineering (ETI)
Karlsruhe Institute of Technology (KIT)
Karlsruhe, Germany
andreas.liske@kit.edu

4th Marc Hiller
Institute of Electrical Engineering (ETI)
Karlsruhe Institute of Technology (KIT)
Karlsruhe, Germany
marc.hiller@kit.edu

***Abstract*—The impedance-based stability criterion has been established as an important tool to assess interactions of power converters with each other and the electrical grid. The converter impedance is strongly influenced by the converter control system, which can include a variety of parameters. This is especially relevant for converters connected to the grid using LCL filters. Additionally, higher switching frequencies extend the frequency range where the converter impedance is affected by the control parameter selection. Insights on how the selection of control parameters shapes the resulting impedance are therefore essential. This paper presents an impedance model of a 50 kHz LCL-connected converter that includes all relevant control parameters. The modeled influences on the converter impedance are verified with measurements of impedance curves with parameter variations. Finally, control parameters are adjusted to shape the impedance and to prevent resonances in a laboratory setup.**

***Index Terms*—Control interaction, converter control, harmonic stability, harmonic impedance measurement, LCL filter**

I. Introduction

The shift towards renewable energy generation and the ongoing electrification lead to a rising penetration of power grids with power electronics. Grid codes require sufficient attenuation of switching harmonics for these converters, which is often accomplished using LCL filters. As this filter structure is prone to resonances, additional active damping measures need to be considered as part of the controller design [1], [2]. Another challenge for the controller design is the uncertainty and variation of the grid impedance at the point of common coupling (PCC). Non-ideal grid strength and conditions can lead to interactions between neighboring converters and between converters and the grid. These interactions result in undesired harmonic resonances, as evidenced in real-world incidents [3], [4]. The impedance-based stability criterion has gained interest in research and standardization drafts because of its ability to be applied using measured black-box models of individual converters and its insights into individual contributions to the system stability [5]–[7]. Knowledge about the converter impedance is therefore critical to assess converter interactions. Impedance modeling approaches, as well as impedance measurement methods are already focus of related works [8], [9]. As the impedance is strongly influenced by the control system of the converter, the effect of control parameter variation on the resulting impedance warrants particular focus [10]–[13], such as the trade-offs regarding the feed-forward of the PCC voltage [14], [15]. The multitude of possible control parameter combinations consequently translates into a wide range of resulting converter impedance curves. Additionally, with the introduction of fast-switching wide-bandgap semiconductors and high-performance control implementations, the frequency range affected by the selection of control parameters is increased as well. In this paper, the existing research is extended by considering a converter with high switching and sampling frequency of $50\,\mathrm{kHz}$ based on SiC-MOSFETs, together with an LCL filter with a resonant frequency of $7.5\,\mathrm{kHz}$. For the control system, combinations of a range of parameters are investigated for both grid current and converter current feedback. A main focus of this paper is to verify the modeled influences on the converter impedance by impedance measurements, demonstrating also the black-box capability of the impedance-based approach. Finally, the modeled and measured converter impedance is used to assess observed resonances and to adjust the control parameters accordingly.

II. Converter Impedance

This section briefly introduces the impedance-based stability criterion before presenting the system under study including its control structure. The control structure is then translated into a

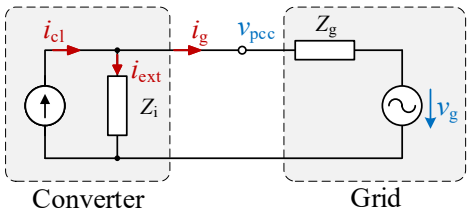

Fig. 1. Impedance model of the converter-grid system

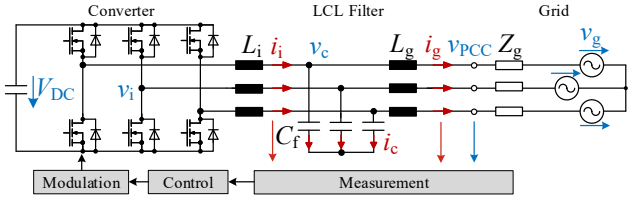

Fig. 2. Converter with LCL filter and signal processing

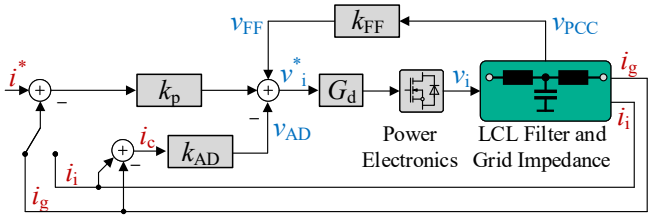

Fig. 3. Converter control structure

signal flow graph, which is used to derive converter impedance models including all considered control parameters.

A. Impedance-Based Stability

The converter current control design mainly deals with the feedback loop that is closed when the measured current is compared to its setpoint. But even if this internal stability is ensured, a non-ideal grid introduces a second feedback loop that can cause instabilities. This interaction can be analyzed if the converter current response to external voltage disturbances is modeled as an impedance, i.e. $i_{\mathrm{ext}} = v_{\mathrm{PCC}}/Z_{\mathrm{i}}$. This model is shown in Fig. 1. The total current at the point of common coupling i_{g} then consists of a component resulting from the closed-loop current control i_{cl} and the aforementioned external current i_{ext} caused by PCC voltage disturbances. The PCC voltage v_{PCC} can then be determined as follows:

$$\begin{aligned} v_{\mathrm{PCC}} &= v_{\mathrm{g}} + Z_{\mathrm{g}} i_{\mathrm{g}} \\ &= v_{\mathrm{g}} + Z_{\mathrm{g}}(i_{\mathrm{cl}} - i_{\mathrm{ext}}) \\ &= v_{\mathrm{g}} + Z_{\mathrm{g}}(i_{\mathrm{cl}} - v_{\mathrm{PCC}}/Z_{\mathrm{i}}) \end{aligned}$$

$$v_{\mathrm{PCC}} = (v_{\mathrm{g}} + Z_{\mathrm{g}} i_{\mathrm{cl}}) \frac{1}{1 + Z_{\mathrm{g}}/Z_{\mathrm{i}}} \tag{1}$$

This derivation reveals the feedback loop created by the grid and converter impedance. Additionally, the standard form of the closed feedback loop allows to employ conventional stability criteria such as the Nyquist criterion. The external stability can be assessed by considering the open-loop transfer function T, which is given by the ratio of the converter and grid impedance $T = Z_{\mathrm{g}}/Z_{\mathrm{i}}$. Thus, the critical points of T are those where $|Z_{\mathrm{g}}| \geq |Z_{\mathrm{i}}|$ and $\angle Z_{\mathrm{g}} - \angle Z_{\mathrm{i}} = (2n+1)\pi$, $n \in \mathbb{Z}$ applies.

B. Converter Impedance Model

The considered system is shown in Fig. 2. It consists of a two-level converter connected to the grid using an LCL filter. The relevant system parameters are given in Table I with the LCL resonant frequency ω_{LCL} and the grid-side LC resonant frequency ω_{LC} defined as

$$\omega_{LCL} = \sqrt{\frac{L_{\mathrm{i}} + L_{\mathrm{g}}}{L_{\mathrm{i}} L_{\mathrm{g}} C_{\mathrm{f}}}} \quad \text{and} \quad \omega_{LC} = \frac{1}{\sqrt{L_{\mathrm{g}} C_{\mathrm{f}}}}. \tag{2}$$

The converter control structure is presented in Fig. 3. A switch before the current error calculation allows to control either the grid current i_{g} or the converter current i_{i}. Control parameters are the proportional gain k_{p}, the active damping gain k_{AD} based on the capacitor current i_{c}, the PCC voltage feed-forward gain k_{FF} and the delay $G_{\mathrm{d}} = e^{-T_{\mathrm{d}} s}$. As the focus of this paper is on the frequency range above 1 kHz, the presented model in the $\alpha\beta$-domain neglects the resonant controller parts at the fundamental and harmonic frequencies, as well as the outer loops of the phase-locked loop (PLL) and DC voltage control. No frequency coupling effects are considered, as the assumed model is symmetric.

In order to determine the converter impedance resulting from this control structure together with the LCL filter dynamics, Mason's gain formula is employed. The required system signal flow graph is shown in Fig. 4. This yields the

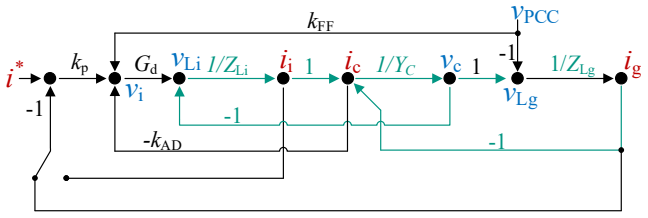

Fig. 4. Signal flow graph of controller and physical system

TABLE I
RELEVANT SYSTEM PARAMETERS

Parameter	Symbol	Value
Converter-side LCL inductance	L_{i}	100 µH
Grid-side LCL inductance	L_{g}	50 µH
LCL filter capacitance	C_{f}	13.5 µF
Switching and sampling frequency	f_{sw}	50 kHz
DC link voltage	V_{DC}	600 V
LCL resonant frequency	ω_{LCL}	7.5 kHz
LC resonant frequency	ω_{LC}	6.1 kHz

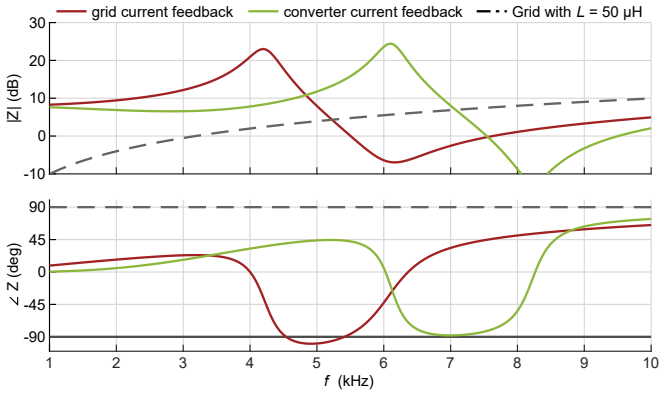

Fig. 5. Modeled converter impedances for grid and converter current feedback

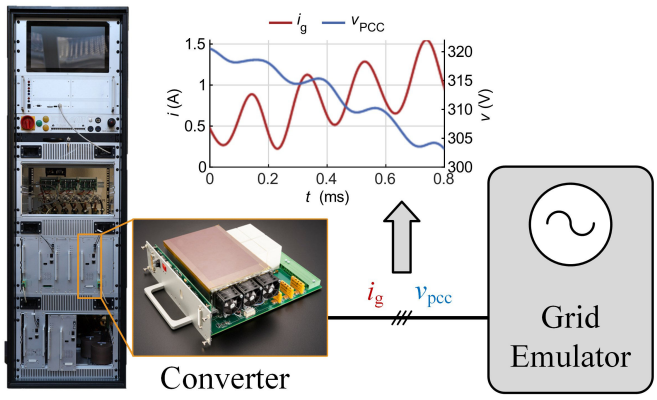

Fig. 6. Impedance measurement setup

following expressions for the converter impedance Z_{i_i} when using converter current feedback and Z_{i_g} for grid current feedback:

$$Z_{i_\mathrm{i}} = \frac{V_\mathrm{PCC}(s)}{-I_g(s)} = \frac{Z_\mathrm{i}Z_\mathrm{g}Y_\mathrm{c} + (k_\mathrm{p}+k_\mathrm{AD})G_\mathrm{d}Z_\mathrm{g}Y_\mathrm{c} + (Z_\mathrm{i}+Z_\mathrm{g}) + k_\mathrm{p}G_\mathrm{d}}{Z_\mathrm{i}Y_\mathrm{c} + (k_\mathrm{p}+k_\mathrm{AD})G_\mathrm{d}Y_\mathrm{c} - k_\mathrm{FF}G_\mathrm{d} + 1} \tag{3}$$

$$Z_{i_\mathrm{g}} = \frac{V_\mathrm{PCC}(s)}{-I_g(s)} = \frac{Z_\mathrm{i}Z_\mathrm{g}Y_\mathrm{c} + k_\mathrm{AD}G_\mathrm{d}Z_\mathrm{g}Y_\mathrm{c} + (Z_\mathrm{i}+Z_\mathrm{g}) + k_\mathrm{p}G_\mathrm{d}}{Z_\mathrm{i}Y_\mathrm{c} + k_\mathrm{AD}G_\mathrm{d}Y_\mathrm{c} - k_\mathrm{FF}G_\mathrm{d} + 1} \tag{4}$$

with

$$\begin{aligned} Z_\mathrm{i} &= sL_\mathrm{i} + R_\mathrm{i} \\ Z_\mathrm{g} &= sL_\mathrm{g} + R_\mathrm{g} \\ Y_\mathrm{c} &= sC_\mathrm{f} \,||\, \frac{1}{R_\mathrm{c}} \\ G_\mathrm{d} &= e^{-T_\mathrm{d}s} \end{aligned}$$

Equations (3) and (4) contain all considered control parameters. The derived model also allows to include additional signal delays and filters present in the real system by adjusting the path gains, for example $k'_\mathrm{FF}(s) = k_\mathrm{FF} \cdot H_\mathrm{meas}(s)$. Typical measurement dynamics include a time delay T_meas and a low-pass characteristic with a cut-off frequency f_meas. These can be described as

$$H_\mathrm{meas} = \frac{2\pi f_{meas}}{2\pi f_{meas} + s}\, e^{-T_{meas}s}. \tag{5}$$

Fig. 5 shows converter impedance curves determined with (3) and (4) for grid current i_g and converter current i_i feedback with proportional gain $k_\mathrm{p} = 2$. Also shown is the impedance of a strong inductive grid with $L = 50\,\mu\mathrm{H}$. Together the curves indicate critical frequencies of 5 kHz for grid current feedback and 7 kHz for converter current feedback.

III. Measurements of Converter Impedances and Resonances

This section describes the laboratory setup to perform the converter impedance measurements. Measurement results are then shown for grid-current feedback and converter-current feedback. Finally, the modeled and measured converter impedances are used to assess observed resonances.

A. Measurement Setup

The control structure presented in Sec. II is implemented on an Artix™-7 FPGA. All discussed control parameters can be tuned online, as well as the selection of the feedback current. The total signal delay is $T_\mathrm{d} = 2\,T_\mathrm{sw} = 2/f_\mathrm{sw}$ and consists of one computation time step, as well as half a time step delay for the modulation and input oversampling each. A flag can be set to delay all measurements by one additional computation time step T_sw. The FPGA implementing the control is combined with a power electronics stage based on SiC-MOSFETs to form the considered converter system [16], which is shown in Fig. 6. An Egston Power CSU100 grid emulator is employed to emulate a 400 V / 50 Hz grid. Additionally, this emulator is programmed to excite the connected converter with voltage disturbances. Sinusoidal positive-sequence disturbances at multiples of the fundamental frequency ranging from 1 kHz to 10 kHz are applied for 200 ms each. The amplitude of the disturbance is adjusted between 500 mV and 1 V according to the expected converter impedance to limit the resulting currents. The grid voltage and the grid currents are measured and transformed into the frequency domain, where the impedance can then be determined as $Z(f) = V_\mathrm{PCC}(f)/I_\mathrm{g}(f)$. Fig. 6 shows the complete measurement setup.

The impedance measurement setup and the tunable control parameters enable the measurement of the influence of individual control parameters while maintaining all other control and system parameters constant. When choosing $n_\mathrm{d} = 1$, all measurements are delayed by one additional sampling period, such that $T_d = (2 + n_\mathrm{d})T_\mathrm{sw}$ and $G_\mathrm{d} = e^{-(2+n_\mathrm{d})T_\mathrm{sw}s}$. If not otherwise specified, the default control parameters listed in Table II are used.

TABLE II
DEFAULT CONTROL AND GRID PARAMETERS

k_p	k_FF	k_AD	n_d	L_grid
2	0	0	0	50 µH

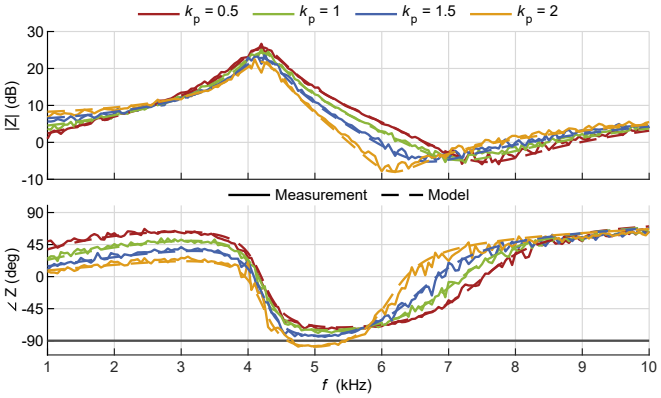

Fig. 7. Impedance Z_{i_g} with variation of proportional control gain k_p

B. Grid Current Feedback

In Fig. 7, the converter impedance for grid current feedback is measured with $k_\mathrm{AD} = k_\mathrm{FF} = 0$ and no additional signal delay. The proportional control gain k_p is varied between 0.5 and 2. The measurements show a good match with the impedance model plotted in a dashed line. The influence of the proportional gain k_p is visible: For higher k_p, the impedance magnitude and thus disturbance rejection is higher at lower frequencies. Conversely, the impedance phase $\angle Z_\mathrm{i}$ is reduced below $-90°$ at $f \approx 5\,\mathrm{kHz}$, which together with an inductive grid impedance results in a critical angle of $\angle \frac{Z_\mathrm{grid}}{Z_\mathrm{i}} \geq 180°$.

In Fig. 8, the measured converter impedance is shown for grid current feedback with variation of the feed-forward gain k_FF between 0 and 1. With rising k_FF, the impedance magnitude increases at lower frequencies, indicating better disturbance rejection. Additionally, the resonant peak around 4 kHz disappears and the impedance phase minimum increases up to $\angle Z \geq -45°$. In turn, the impedance phase reaches

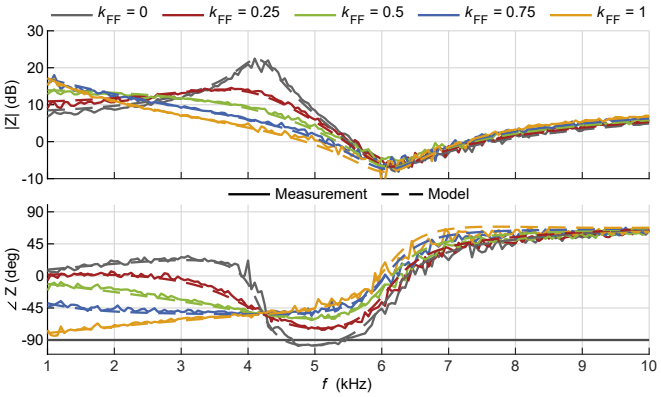

Fig. 8. Impedance Z_{i_g} with variation of feed-forward gain k_FF

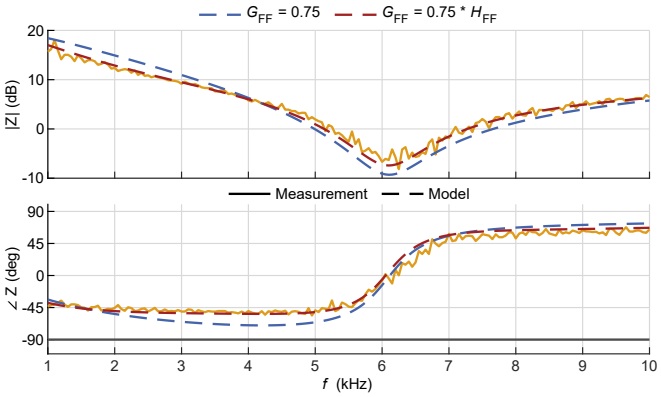

Fig. 9. Effect of measurement delay modeling on converter impedance Z_{i_g} with feed-forward gain $k_\mathrm{FF} = 0.75$

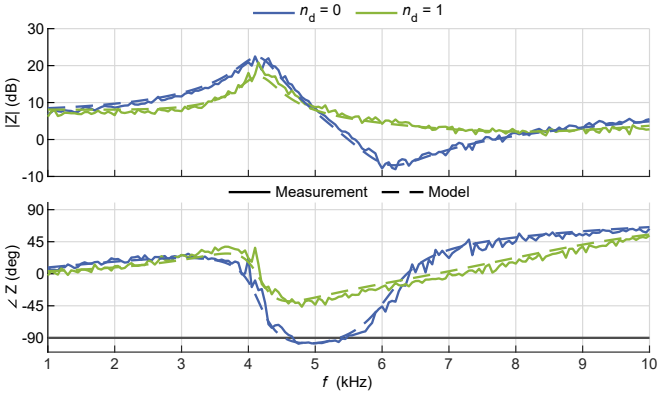

Fig. 10. Impedance Z_{i_g} with feed-forward gain $k_\mathrm{FF} = 0$ and variation of additional delay step n_d

critically low values at lower frequencies around 1 kHz for $k_\mathrm{FF} = 1$, which can lead to problems in weak grids.

Fig. 9 shows the importance of accurate modeling of signal delays. The PCC voltage measurement on the power stage introduces an additional sensor delay of $T_{v_\mathrm{PCC}} = 5\,\mu\mathrm{s}$ and a low-pass characteristic with a cut-off frequency of $f_{v_\mathrm{PCC}} = 30\,\mathrm{kHz}$. The curves in Fig. 9 show the converter impedance for grid-current feedback with partial voltage feed-forward $k_\mathrm{FF} = 0.75$. The curves demonstrate that neglecting the measurement dynamics results in a modeled minimum impedance phase of $\angle Z \approx -70°$ shown in the dashed blue line, while the measured impedance has a phase of $\angle Z \approx -50°$. When the measurement dynamics described by (5) are included in the model as described in Sec. II, the impedance curve plotted in red shows a good match with the measured impedance. For the considered hardware, other measurement dynamics have been determined to be negligible.

Fig. 10 and Fig. 11 show the influence of an additional delay when using grid current feedback. Fig. 10 shows the converter impedance for $k_\mathrm{p} = 2$ and disabled PCC voltage feed-forward. Enabling the additional delay step eliminates the resonance minimum and lifts the phase minimum from $\angle Z < -90°$ to $\angle Z \geq -45°$. Fig. 11 shows the converter

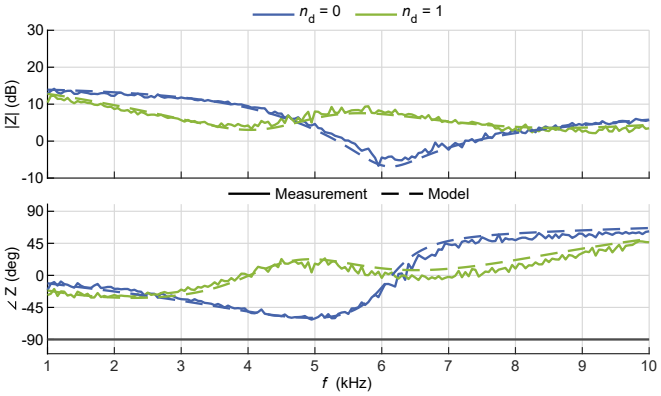

Fig. 11. Impedance Z_{i_g} with feed-forward gain $k_{FF} = 0.5$ and variation of additional delay step n_d

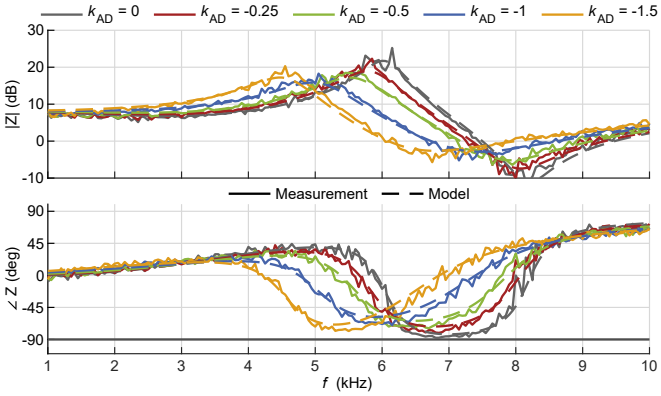

Fig. 13. Impedance Z_{i_i} with variation of active damping gain k_{AD}

impedance for $k_p = 2$ and enabled PCC voltage feed-forward with $k_{FF} = 0.5$. Again, the additional delay eliminates the magnitude minimum and increases the phase minimum. The measurements also demonstrate the control influence up to 10 kHz. For higher frequencies, the impedance curves all converge to the passive behaviour of the grid-side filter inductance L_g including ohmic and frequency-dependent losses.

C. Converter Current Feedback

Fig. 12 shows converter impedance measurements with converter current feedback, $k_{AD} = k_{FF} = 0$ and no additional signal delay. The proportional control gain k_p is varied between 0.5 and 2. For higher k_p the resonant peak in the impedance magnitude moves to higher frequencies and the minimum impedance phase $\angle Z_i$ approaches $-90°$. Compared to the converter impedance with grid current feedback using the same control parameters in Fig. 7, the impedance magnitude in Fig. 12 peaks near the LC resonant frequency $\omega_{LC} = 6.1$ kHz and reaches a minimum around the LCL resonant frequency of $\omega_{LCL} = 7.5$ kHz. The direct comparison is visible in the modeled impedance curves in Fig. 5.

In Fig. 13, the active damping gain k_{AD} is varied between 0 and -1.5. The negative sign results from the convention

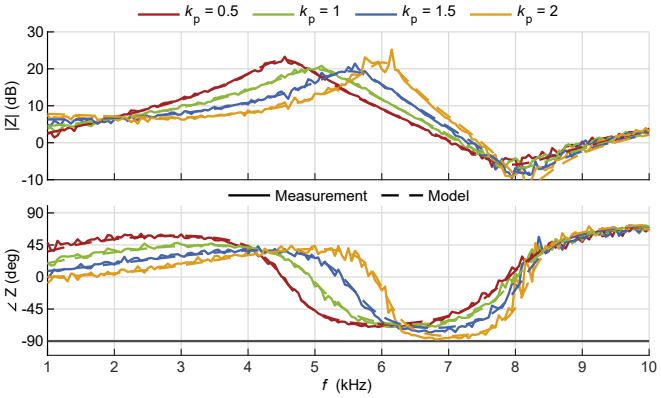

Fig. 12. Impedance Z_{i_i} with variation of proportional control gain k_p

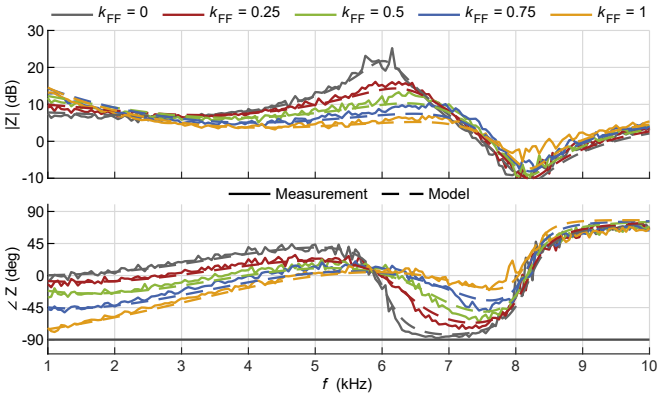

Fig. 14. Impedance Z_{i_i} with variation of feed-forward gain k_{FF}

indicated in Fig. 3. For rising values of $|k_{AD}|$, the resonant amplitude peak moves to lower frequencies. The phase minimum is highest for $k_{AD} = -1$ before falling again for $k_{AD} = -1.5$, where the control almost transitions into grid-current feedback.

Fig. 14 shows converter impedance measurements for converter current feedback where the feed-forward gain k_{FF} is varied between 0 and 1. Similar to the influence for grid current feedback in Fig. 8, higher values of k_{FF} increase the phase margin at higher frequencies around 8 kHz, but introduce critical phase margin at lower frequencies around 1 kHz. The selection of $k_{FF} = 0.5$ appears to offer a sensible trade-off for both grid and converter current feedback. This is visible in more detail in Table III, where the phase margin is defined as PM $= 180° - (\angle Z_g - \angle Z_i) = 90° + \angle Z_i$ for an inductive grid with $\angle Z_g = 90°$.

TABLE III
EFFECT OF PCC VOLTAGE FEED-FORWARD ON PHASE MARGIN AT CRITICAL FREQUENCIES

k_{FF}	PM for grid current i_g		PM for converter current i_i	
	@1 kHz	@5 kHz	@1 kHz	@7 kHz
0	99°	−7°	90°	5°
0.5	79°	30°	68°	50°
1	10°	44°	15°	85°

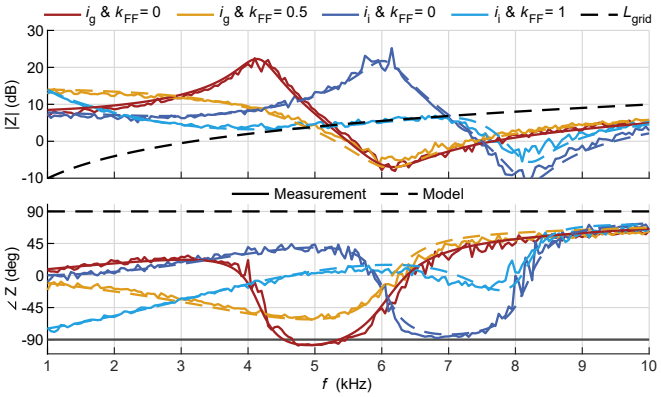

Fig. 15. Impedances Z_{i_g} and Z_{i_i} with variation of feed-forward gain k_{FF}

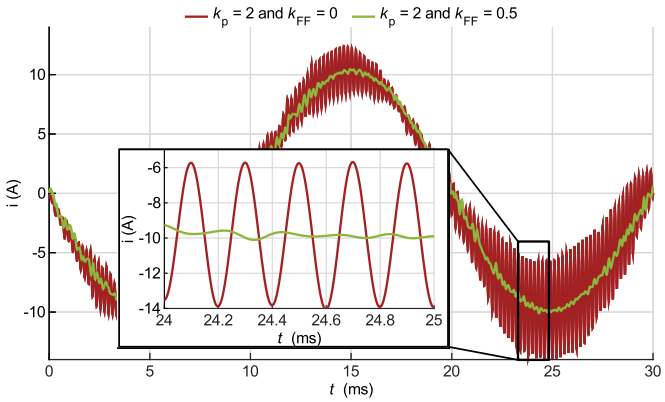

Fig. 16. Time-domain measurement of resonance with grid current feedback

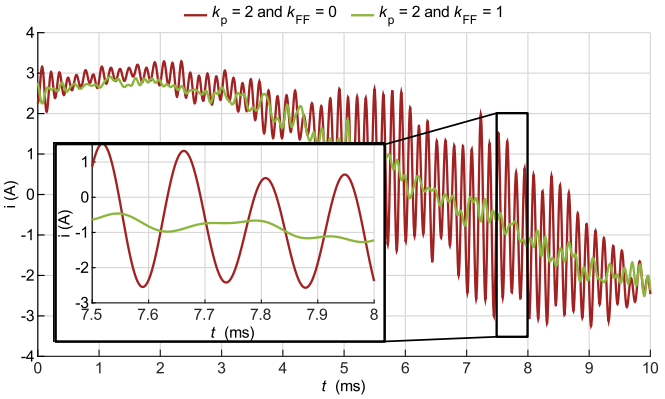

Fig. 17. Time-domain measurement of resonance with converter current feedback

D. Resonances at Critical Impedance Ratios

In order to further verify the measured impedance curves and the resulting stability assessments, this subsection shows time-domain measurements for critical impedance ratios. Fig. 15 shows the converter impedances for grid and converter current feedback with variation of the voltage feed-forward gain k_{FF}. When using grid current feedback and no voltage feed-forward, the grid impedance crosses the converter impedance at around 5 kHz, where the total phase of the impedance ratio reaches $\angle\frac{Z_{grid}}{Z_i} = 180°$, indicating an instability at this frequency. When selecting $k_{FF} = 0.5$, the increased impedance phase avoids an instability. This is visible in Fig. 16, where the associated time-domain measurements with no harmonic voltage excitation are shown. The resonance with a frequency of 5 kHz and an amplitude of up to 4 A disappears after enabling partial voltage feed-forward.

In the case of converter current feedback and disabled voltage feed-forward, the grid impedance crosses the converter impedance at around 7 kHz, where the total phase of the impedance ratio again reaches $\angle\frac{Z_{grid}}{Z_i} = 180°$. Selecting $k_{FF} = 1$ increases the converter impedance phase at that frequency and avoids an instability. The associated time-domain measurements are shown in Fig. 17. The resonance with a frequency of 7 kHz and an amplitude of up to 1.5 A disappears after the voltage feed-forward is enabled.

IV. Conclusion

The presented converter impedance measurements with variations of multiple relevant control parameters demonstrate their significant influence on the impedance in the critical LCL frequency range for both grid current and converter current feedback. Active damping based on capacitor current measurement, additional delay in the case of grid current feedback and proportional PCC voltage feed-forward can all have a beneficial effect on the converter impedance phase at critical LCL frequencies. The developed symmetric $\alpha\beta$-frame impedance model is validated by the close match with the measured impedance curves for the considered frequencies and time-domain measurements of critical resonances as predicted by the modeled and measured converter impedances. The results highlight the importance of considering external control interactions during control parameter selection. The control influence over a wide frequency range up to 10 kHz necessitates detailed modeling of measurement dynamics and further stresses the advantage of verification using black-box measurements.

References

[1] W. Wu, Y. Liu, Y. He, H. S.-H. Chung, M. Liserre, and F. Blaabjerg, "Damping Methods for Resonances Caused by LCL-Filter-Based Current-Controlled Grid-Tied Power Inverters: An Overview," *IEEE Transactions on Industrial Electronics*, vol. 64, no. 9, pp. 7402–7413, Sep. 2017.

[2] G. Shen, X. Zhu, J. Zhang, and D. Xu, "A New Feedback Method for PR Current Control of LCL-Filter-Based Grid-Connected Inverter," *IEEE Transactions on Industrial Electronics*, vol. 57, no. 6, pp. 2033–2041, Jun. 2010.

[3] C. Li, "Unstable Operation of Photovoltaic Inverter From Field Experiences," *IEEE Transactions on Power Delivery*, vol. 33, no. 2, pp. 1013–1015, Apr. 2018.

[4] J. Sun, G. Wang, X. Du, and H. Wang, "A Theory for Harmonics Created by Resonance in Converter-Grid Systems," *IEEE Transactions on Power Electronics*, vol. 34, no. 4, pp. 3025–3029, Apr. 2019. (visited on 03/06/2024).

[5] J. Sun, "Impedance-Based Stability Criterion for Grid-Connected Inverters," *IEEE Transactions on Power Electronics*, vol. 26, no. 11, pp. 3075–3078, Nov. 2011.

[6] L. Harnefors, A. G. Yepes, A. Vidal, and J. Doval-Gandoy, "Passivity-Based Controller Design of Grid-Connected VSCs for Prevention of Electrical Resonance Instability," *IEEE Transactions on Industrial Electronics*, vol. 62, no. 2, pp. 702–710, Feb. 2015.

[7] X. Wang and F. Blaabjerg, "Harmonic Stability in Power Electronic-Based Power Systems: Concept, Modeling, and Analysis," *IEEE Trans. Smart Grid*, vol. 10, no. 3, pp. 2858–2870, May 2019.

[8] G. Francis, R. Burgos, D. Boroyevich, F. Wang, and K. Karimi, "An algorithm and implementation system for measuring impedance in the D-Q domain," in *2011 IEEE Energy Conversion Congress and Exposition*, Sep. 2011, pp. 3221–3228.

[9] H. Gong, X. Wang, and D. Yang, "DQ-Frame Impedance Measurement of Three-Phase Converters Using Time-Domain MIMO Parametric Identification," *IEEE Transactions on Power Electronics*, vol. 36, no. 2, pp. 2131–2142, Feb. 2021.

[10] B. Wen, D. Boroyevich, R. Burgos, P. Mattavelli, and Z. Shen, "Small-Signal Stability Analysis of Three-Phase AC Systems in the Presence of Constant Power Loads Based on Measured d-q Frame Impedances," *IEEE Trans. Power Electron.*, vol. 30, no. 10, pp. 5952–5963, Oct. 2015.

[11] D. Yang, X. Ruan, and H. Wu, "Impedance Shaping of the Grid-Connected Inverter with LCL Filter to Improve Its Adaptability to the Weak Grid Condition," *IEEE Transactions on Power Electron.*, vol. 29, no. 11, pp. 5795–5805, Nov. 2014.

[12] E. Rodriguez-Diaz, F. D. Freijedo, J. M. Guerrero, J.-A. Marrero-Sosa, and D. Dujic, "Input-Admittance Passivity Compliance for Grid-Connected Converters With an LCL Filter," *IEEE Transactions on Industrial Electronics*, vol. 66, no. 2, pp. 1089–1097, Feb. 2019.

[13] D. Schulz, A. Liske, and M. Hiller, "Multi-Parameter Analysis and Measurement of Resonances in Grid-Connected Converters with LCL Filters," in *2023 25th European Conference on Power Electronics and Applications (EPE'23 ECCE Europe)*, Aalborg, Denmark, Sep. 2023, pp. 1–9.

[14] T. Messo, R. Luhtala, A. Aapro, and T. Roinila, "Accurate Impedance Model of Grid-Connected Inverter for Small-Signal Stability Assessment in High-Impedance Grids," in *2018 International Power Electronics Conference*, Niigata, May 2018, pp. 3156–3163.

[15] Z. Yang, S. He, D. Zhou, *et al.*, "Wideband Dissipativity Enhancement for Grid-Following VSC Utilizing Capacitor Voltage Feedforward," *IEEE Journal of Emerging and Selected Topics in Power Electronics*, vol. 11, no. 3, pp. 3138–3151, Jun. 2023.

[16] S. Frank, D. Schulz, L. Stefanski, R. Schwendemann, and M. Hiller, "A standardized and modular power electronics platform for academic research on advanced grid-connected converter control and microgrids," in *2022 24th European Conference on Power Electronics and Applications (EPE'22 ECCE Europe)*, Sep. 2022, pp. 1–9.